NASA TECHNICAL NOTE

NASA TN D-3819

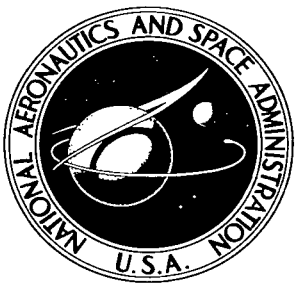

NASA TN D-3819

COLD-AIR PERFORMANCE EVALUATION OF A SCALE-MODEL FUEL PUMP TURBINE FOR THE M-1 HYDROGEN-OXYGEN ROCKET ENGINE

by Roy G. Stabe, John F. Kline, and Edward H. Gibbs

Lewis Research Center
Cleveland, Ohio

NATIONAL AERONAUTICS AND SPACE ADMINISTRATION • WASHINGTON, D. C. • FEBRUARY 1967

NASA TN D-3819

COLD-AIR PERFORMANCE EVALUATION OF A SCALE-MODEL FUEL PUMP TURBINE FOR THE M-1 HYDROGEN-OXYGEN ROCKET ENGINE

By Roy G. Stabe, John F. Kline, and Edward H. Gibbs

Lewis Research Center
Cleveland, Ohio

NATIONAL AERONAUTICS AND SPACE ADMINISTRATION

For sale by the Clearinghouse for Federal Scientific and Technical Information
Springfield, Virginia 22151 – Price $2.00

COLD-AIR PERFORMANCE EVALUATION OF A SCALE-MODEL FUEL PUMP TURBINE FOR THE M-1 HYDROGEN-OXYGEN ROCKET ENGINE

by Roy G. Stabe, John F. Kline, and Edward H. Gibbs

Lewis Research Center

SUMMARY

The aerodynamic performance of a 0.646-scale-model fuel turbopump drive turbine for the M-1 rocket engine was determined experimentally. The working fluid used in the investigation of the two-stage velocity-compounded turbine was dry air at inlet total conditions of 25 psia and 600° R. The turbine inlet manifold assembly was first tested as a separate unit. Two-stage and first-stage turbine configurations, including the inlet manifold, were then tested over a range of speeds and pressure ratios.

The convergent-divergent nozzle choked at a pressure ratio of 1.5, resulting in constant equivalent weight flow over the range of speeds and pressure ratios investigated. The actual equivalent weight flow was 2.88 pounds per second, which was 1.5 percent greater than the design value of 2.837 pounds per second.

Manifold static pressure measurements and circumferential surveys of nozzle exit total pressure indicated a considerable circumferential variation in inlet manifold assembly flow conditions. These variations were largely confined to approximately one-third of the manifold circumference centered about the inlet feedpipe. The loss in total pressure between the feedpipe and nozzle inlet was estimated to be about 5 percent of inlet total pressure or about 1.2 inlet velocity heads.

At design equivalent speed and pressure ratio, the two-stage turbine static efficiency was 0.65 compared to the design value of 0.622. The equivalent specific work was 29.7 Btu per pound, or 4.5 percent greater than design. The first stage produced 71.7 percent of the total work at a static efficiency of 0.51. The design values were 72.3 percent and 0.490, respectively. The total efficiency of the first stage was 0.64 compared to the design value of 0.599.

INTRODUCTION

Experimental performance evaluations of the pump-drive turbines for the M-1 engine have been included as part of the turbine research and project support programs. The M-1 is a 1.5-million-pound-thrust hydrogen-oxygen rocket engine. Fuel and oxidizer turbopumps are mounted on either side of the engine combustion chamber and each is driven by a two-stage velocity-compounded turbine. The two-stage unit was overhung from the turbopump bearings, thus avoiding the complication of an outboard turbine bearing. The nozzle in a velocity-compounded turbine converts virtually all of the energy available to the turbine to velocity, which results in low casing pressure and small pressure changes across the remaining blade rows. This condition results in comparitively low shaft thrust and interstage leakage and lightweight casing design.

Details of the oxidizer pump-drive turbine design may be found in reference 1. Cold-air performance evaluations of a 0.45-scale-model oxidizer turbine manifold assembly and complete two-stage turbine have been reported in references 2 and 3, respectively. Design details of the fuel pump turbine have been reported in reference 4. This report presents the results of a cold-air performance evaluation of a 0.646-scale-model fuel pump-drive turbine.

The feedpipe-manifold-nozzle assembly was first tested as a separate unit. Circumferential surveys of nozzle exit total pressure were made at several feedpipe total to nozzle exit static pressure ratios. Feedpipe, manifold, and nozzle exit static pressure and weight flow data were also taken. The data were taken over a range of pressure ratios from 1.2 to 2.7.

Two-stage and first-stage turbine configurations were then tested at constant speeds of 60, 80, 90, 100, and 105 percent of design equivalent speed and over a range of pressure ratios from 1.5 to 5.0 for the first-stage and 1.5 to 6.0 for the two-stage turbine configurations. Zero-speed torque data were also obtained. Turbine performance in terms of weight flow, specific work, static efficiency, and torque are presented for the range of speeds and pressure ratios covered in the investigation. Interstage static pressure data and the results of radial surveys of rotor exit flow conditions at design equivalent speed and pressure ratio are also included.

SYMBOLS

$\mathcal{A}$ aspect ratio, ratio of maximum blade height to actual chord, maximum x value, table IV

c_p specific heat at constant pressure, Btu/(lb)($^{\circ}$R)

D	diameter, in.
g_c	dimensional conversion constant, 32.17 (ft-lb)/(lb)(sec^2)
$\Delta h'$	specific work, Btu/lb
J	mechanical equivalent of heat, 778 ft-lb/Btu
N	speed, rpm
P	power, hp
p	pressure, lb/sq in. abs
R	gas constant, ft-lb/(lb)(^oR)
Re	turbine Reynolds number, $Re = 12w/r_m\mu$
r	radius, in.
S.F.	scale factor, ratio of scale-model to full-size mean diameters
T	temperature, ^oR
U	blade speed, ft/sec
V	absolute velocity, ft/sec
W	velocity relative to rotor blade, ft/sec
w	weight flow, lb/sec
α	absolute flow angle, deg from axial
β	relative flow angle, deg from axial
γ	ratio of specific heats
δ	ratio of inlet total pressure to NACA standard atmosphere pressure, $p'_1/14.696$
ϵ	gamma correction function, $\frac{0.740}{\gamma}\left(\frac{\gamma+1}{2}\right)^{\gamma/(\gamma-1)}$
η	static efficiency, based on total to static pressure ratio across turbine
η'	total efficiency, based on total to total pressure ratio across turbine
$\sqrt{\theta_{cr}}$	ratio of turbine inlet critical velocity to critical velocity of NACA standard air, $V_{cr,1}/1019.46$
μ	absolute viscosity, lb/(ft)(sec)
υ	blade-jet speed ratio, $U_m \Big/ \sqrt{2g_c J c_p T'_1\left[1-\left(\frac{p_{exit}}{p'_1}\right)^{(\gamma-1)/\gamma}\right]}$

σ	solidity, ratio of actual blade chord (maximum x value, table IV) to blade spacing at the mean diameter
τ	torque, lb-ft

Subscripts:

cr	conditions corresponding to those at Mach number of 1
eq	equivalent
exit	rotor exit, stations 4 or 7
h	blade hub section
m	blade mean section
max	maximum value
t	blade tip section
1, 2, 3, 4, 5, 6, 7	measuring stations (see fig. 8)

Superscripts:

$-$	average value
$'$	absolute total state condition
$''$	total state condition relative to rotor blade

DESCRIPTION OF M-1 FUEL TURBOPUMP DRIVE TURBINE

A mockup of the M-1 engine showing the arrangement of the fuel turbopump, gas generator, and associated ducting is shown in figure 1. Liquid propellant is combusted in the gas generator at an oxidant to fuel mixture ratio of 0.8. Gas from the generator flows through a short feedpipe directly into the toroidal inlet manifold of the fuel turbine, through the turbine into a hemispherically shaped exhaust housing, and then through two ducts which lead to the oxidizer turbine inlet. Figure 2 is a sectioned view of the fuel turbopump showing the internal arrangement of the various components.

The fuel turbopump drive turbine, or fuel turbine, is a two-stage velocity-compounded (Curtis type) machine with a nominally constant mean diameter of 23.175 inches at operating temperature and speed. The mean diameter free stream velocity diagrams are given in figure 3. The nozzle exit and first-stage rotor relative inlet velocities are supersonic. All other velocities are subsonic. The turbine working fluid thermodynamic properties are listed in table I and the design performance specifications

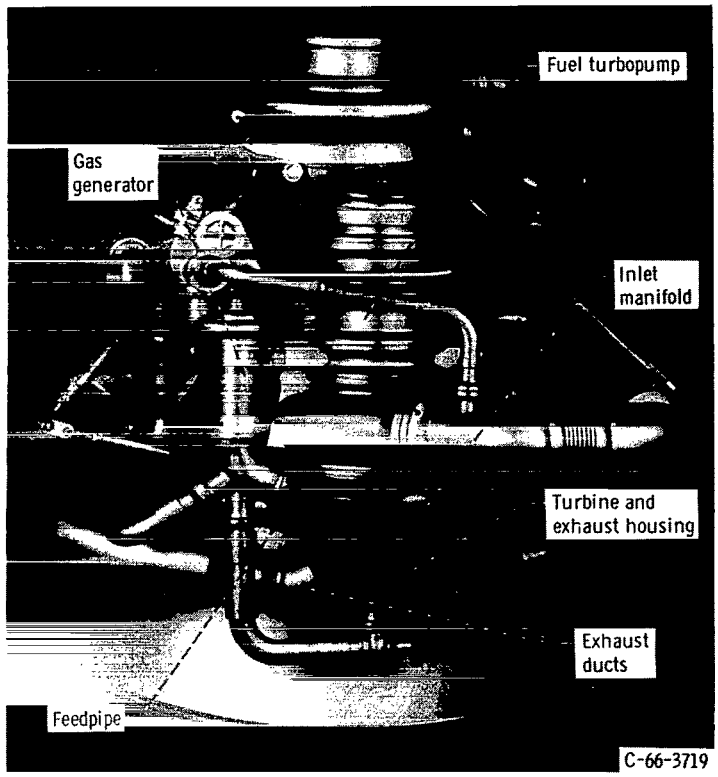

Figure 1. - Fuel turbopump mounted on M-1 engine.

TABLE I. - M-1 FUEL TURBINE THERMODYNAMIC PROPERTIES

	Hydrogen-oxygen combustion products	NACA standard air
Specific heat, c_p, Btu/(lb)(^{o}R)	2.01	0.24
Ratio of specific heats, γ	1.37	1.4
Gas constant, R, ft-lb/(lb)(^{o}R)[a]	422.3	53.35

[a] $R \equiv J(\gamma - 1)c_p/\gamma$.

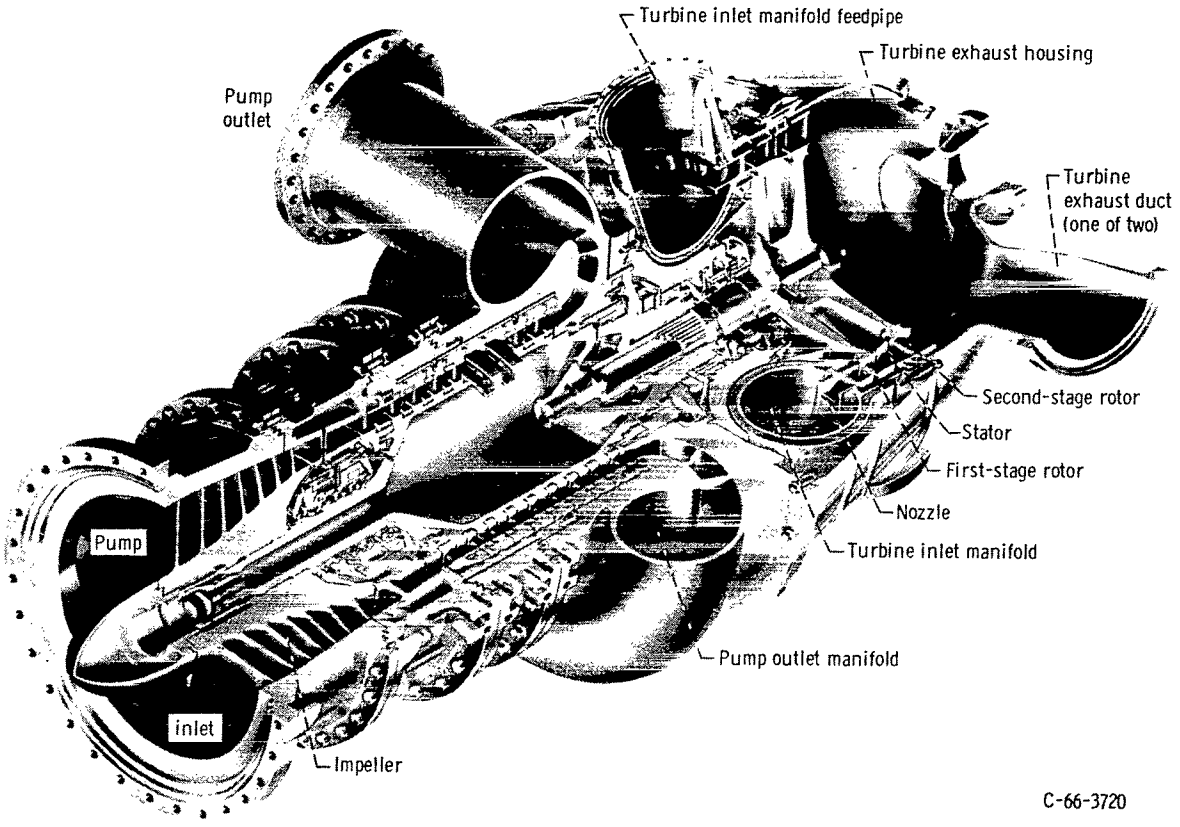

Figure 2. - Fuel turbopump.

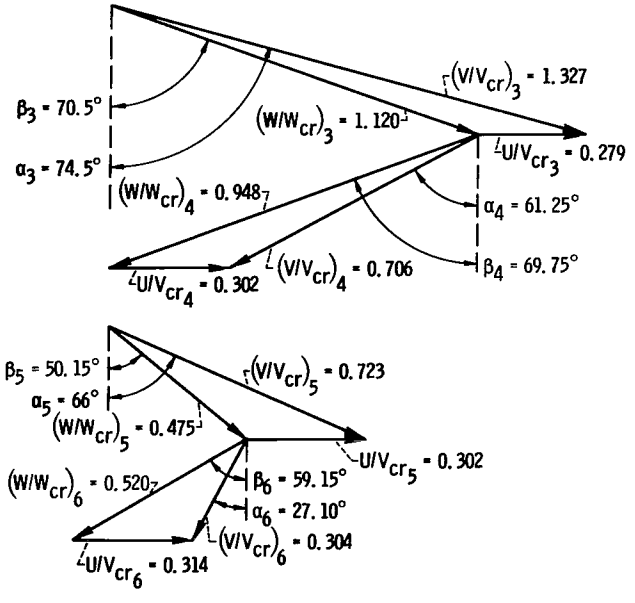

Figure 3. - Design velocity diagrams at mean diameter.

TABLE II. - M-1 FUEL TURBINE DESIGN CONDITIONS

Parameter	Hydrogen-oxygen combustion products		NACA standard air equivalent conditions		
	Symbol	Full size	Symbol	Full size	0.646 Scale
Inlet total temperature, ^{o}R	T'_1	1460	T'_1	518.7	518.7
Inlet total pressure, psia	p'_1	1020	p'_1	14.696	14.696
Mean diameter, in.	D_m	23.175	D_m	23.175	14.963
Weight flow, lb/sec	w	99.33	$w\sqrt{\theta_{cr}}\,\epsilon/\delta$	6.808	2.837
Speed, rpm	N	13 225	$N/\sqrt{\theta_{cr}}$	2815.4	4360.5
Specific work, Btu/lb	$\Delta h'$		$\Delta h'/\theta_{cr}$		
Two stage		627.24		28.428	28.428
One stage		453.76		20.566	20.566
Power, hp	P		$P\epsilon/\delta\sqrt{\theta_{cr}}$		
Two stage		88 131		273.74	114.09
One stage		63 756		198.03	82.539
Torque, lb-ft	τ		$\tau\epsilon/\delta$		
Two stage		35 000		510.66	137.41
One stage		25 320		369.42	99.41
Pressure ratio					
Two stage	$p'_1/\bar{p}_{6,m}$	4.766	$p'_1/\bar{p}_{6,m}$	4.968	4.968
One stage	$p'_1/\bar{p}_{4,m}$	4.080	$p'/\bar{p}_{4,m}$	4.221	4.221
Blade-jet speed ratio	ν		ν		
Two stage		0.188		0.188	0.188
One stage		0.196		0.196	0.196
Static efficiency	η		η		
Two stage		0.622		0.622	0.622
One stage		0.490		0.490	0.490
Total efficiency	η'		η'		
Two stage		0.640		0.640	0.640
One stage		0.599		0.599	0.599

of the turbine, including the inlet manifold, are listed in table II. The specific work, efficiency, torque, and power listed in table II have been derated from the values derived from the velocity diagrams to account for the loss due to flow leakage through the clearance spaces around the blade rows. Other aerodynamic design details may be found in reference 4. NACA standard air equivalent performance parameters for both full-size and scale-model turbines have also been listed in table II. The equivalent turbine performance parameters for the scale-model fuel turbine are related to those of the full-size machine by power functions of the scale factor (S. F.). The design point values were computed as follows:

$$\text{Scale-model equivalent parameter} = \text{Full-size equivalent parameter} \times (\text{S. F.})^{m}$$

The exponent m for each of the various equivalent parameters is as follows: N_{eq}, -1; $\Delta h'_{eq}$, 0; w_{eq}, 2; P_{eq}, 2; and τ_{eq}, 3.

General characteristics of the four blade rows are given in table III. All blades are of nontwisted constant section with some curvature on the suction surfaces downstream of the throat. The rotor blades were slightly tilted from radial to minimize combined blade stresses. The nozzle is a convergent-divergent supersonic design with an exit to throat area ratio of 1.25. All other blade rows are convergent in the guided channels.

A sketch of the fuel turbine is shown in figure 4. Blade heights were increased in each succeeding row to satisfy flow area requirements. Both rotors are shrouded and have cylindrical end walls as does the nozzle. The stator end walls diverge.

TABLE III. - BLADE DESIGN CHARACTERISTICS

Blade row	Number of blades	Radius ratio, r_h/r_t	Solidity, σ	Aspect ratio, $\mathcal{A}$	Free stream turning, deg
Nozzle	37	0.879	1.770	0.428	74.5
First-stage rotor	80	.860	1.508	1.266	140.25
Second-stage stator	67	.818	1.306	1.631	127.25
Second-stage rotor	78	.796	1.734	1.628	109.3

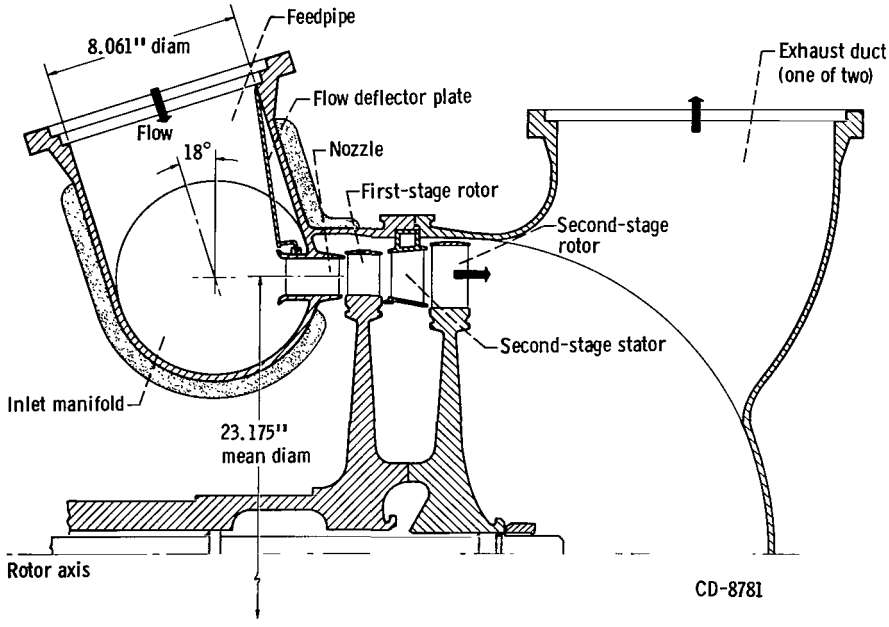

Figure 4. - Schematic of M-1 model III fuel turbine.

DESCRIPTION OF SCALE-MODEL TEST TURBINE

A 0.646 scale model of the M-1 fuel turbine was constructed for the cold-air performance evaluation described herein. The scale factor resulted from the choice of a 14.963-inch mean diameter so that the test turbine could utilize the same test facility, casing, and running gear as the scale-model oxidizer turbine of references 2 and 3.

Turbine testing with scale models and with cold air is a well established technique and yields valid results because of the high degree of similitude obtainable. Reynolds number, however, cannot always be duplicated in this type of test. Reference 5 shows the effect of Reynolds number Re on turbine performance to be negligible for turbine Reynolds numbers greater than 2×10^5. The Reynolds number of the scale-model fuel turbine, as tested, is approximately 5.3×10^5. This value is much lower than the Reynolds number of the full-size machine, which was approximately 74×10^5, but it is high enough to preclude any Reynolds number effects on performance.

A sketch of the scale-model fuel turbine is shown in figure 5. Some deviations from exact similarity between the full-size and scale-model turbines were permitted to simplify manufacture. A comparison of figure 5 with figure 4 illustrates these differences. The hemispherically shaped exhaust section with the two exhaust ducts of the full-size turbine was not included in the evaluation but was replaced with a conically shaped exhaust pipe.

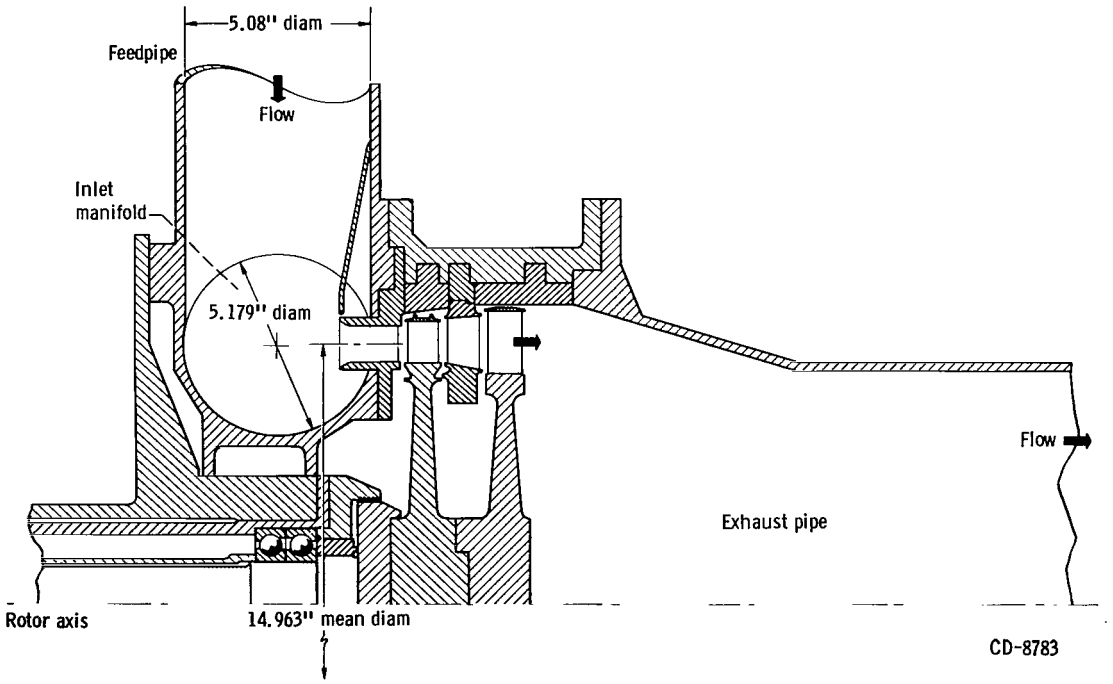

Figure 5. - Schematic of 0.646-scale-model turbine.

TABLE IV. - SCALE-MODEL TURBINE BLADE COORDINATES

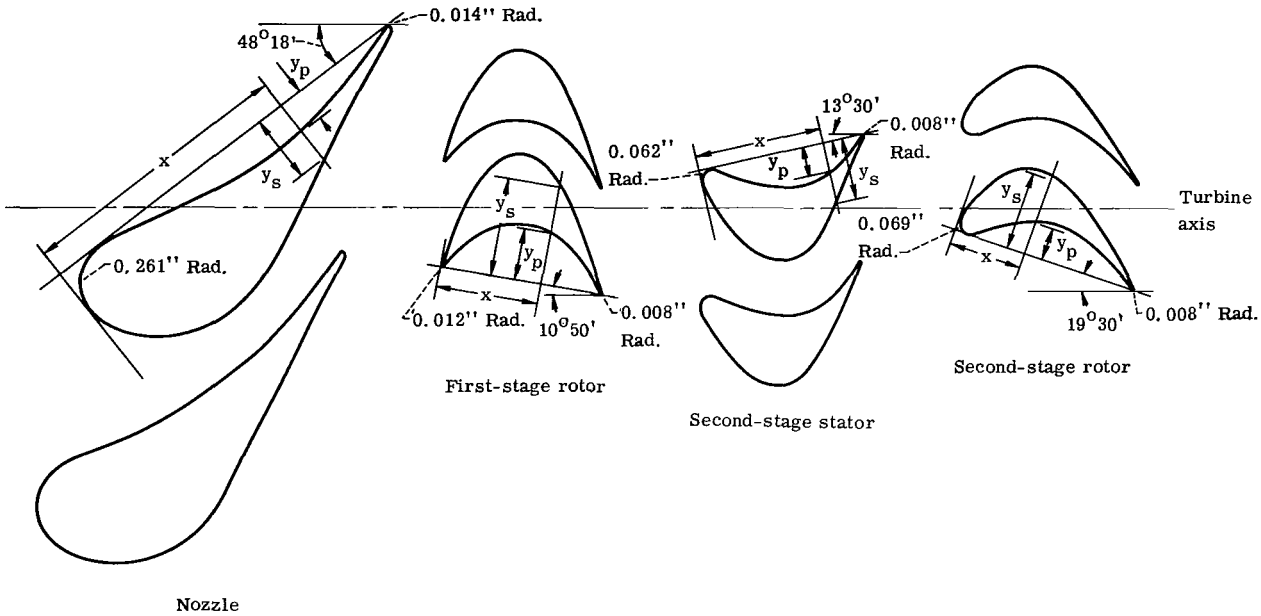

Nozzle coordinates		
x, in.	y_p, in.	y_s, in.
0	-----	0.266
.100	0.056	.498
.200	.007	.602
.300	.003	.681
.400	.027	.716
.500	.051	.741
.600	.074	.749
.700	.098	.743
.800	.122	.722
.900	.141	.691
1.000	.156	.647
1.100	.167	.596
1.200	.172	.546
1.300	.176	.497
1.400	.174	.447
1.500	.169	.396
1.600	.160	.346
1.700	.146	.298
1.800	.129	.247
1.900	.107	.198
2.000	.080	.148
2.100	.049	.097
2.200	.013	.047
2.247	-----	.014

First-stage rotor coordinates		
x, in.	y_p, in.	y_s, in.
0	-----	0.012
.050	0.065	.291
.100	.140	.460
.150	.194	.565
.200	.234	.631
.250	.263	.666
.300	.282	.680
.350	.295	.682
.400	.300	.671
.450	.300	.648
.500	.294	.611
.550	.281	.561
.600	.261	.496
.650	.235	.420
.700	.200	.336
.750	.157	.250
.800	.104	.164
.850	.036	.078
.888	-----	.008

Second-stage stator coordinates		
x, in.	y_p, in.	y_s, in.
0	-----	0.062
.050	0.001	.237
.100	.014	.350
.150	.052	.440
.200	.089	.507
.250	.122	.545
.300	.150	.566
.350	.172	.575
.400	.187	.573
.450	.196	.560
.500	.200	.534
.550	.198	.488
.600	.191	.430
.650	.178	.368
.700	.158	.302
.750	.133	.234
.800	.098	.166
.850	.055	.098
.900	.002	.031
.914	-----	.008

Second-stage rotor coordinates		
x, in.	y_p, in.	y_s, in.
0	-----	0.069
.050	0.003	.242
.100	.007	.325
.150	.051	.387
.200	.093	.431
.250	.127	.458
.300	.155	.471
.350	.177	.474
.400	.193	.466
.450	.203	.450
.500	.208	.429
.550	.209	.403
.600	.204	.373
.650	.195	.339
.700	.180	.302
.750	.163	.262
.800	.142	.221
.850	.117	.178
.900	.089	.135
.950	.058	.093
1.044	-----	.008

Blade shapes and blade profile and positioning coordinates for the scale-model fuel turbine are presented in table IV. The blades were fabricated by electrical discharge machining to a surface finish of 60 microinches. The scale-model rotor blades were not tilted as they were in the full-size machine. Deviations from specified dimensions during manufacture of the scale-model blading resulted in throat area discrepancies given in table V. In addition, the nozzle exit area was undersize, which resulted in a nozzle exit to throat area ratio of 1.172 compared to 1.25 design. It was recognized that these discrepancies prevented exact simulation of the full-size turbine and would affect the turbine flow conditions. They were judged to be of insufficient magnitude, however, to affect the general level of performance.

TABLE V. - THROAT AREA DISCREPANCIES

Blade row	Deviation in throat area from design, percent
Nozzle	1.55 - oversize
First-stage rotor	3.10 - undersize
Second-stage stator	2.73 - undersize
Second-stage rotor	1.57 - undersize

The scale-model first- and second-stage rotors, with the shrouds removed, are shown in figures 6(a) and (b), respectively. The turbine assembly with half of the casing removed is shown in figure 6(c).

A feedpipe-manifold-nozzle configuration (rotors and stator removed) and a one-stage configuration (second

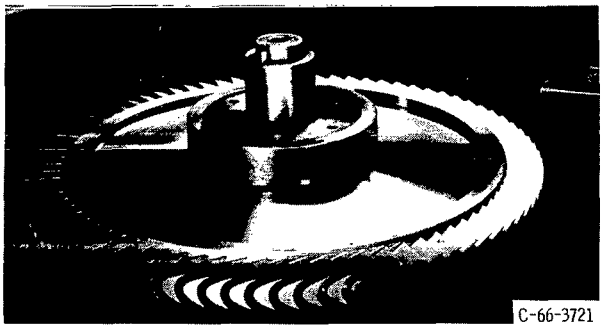

(a) First-stage rotor without tip shroud.

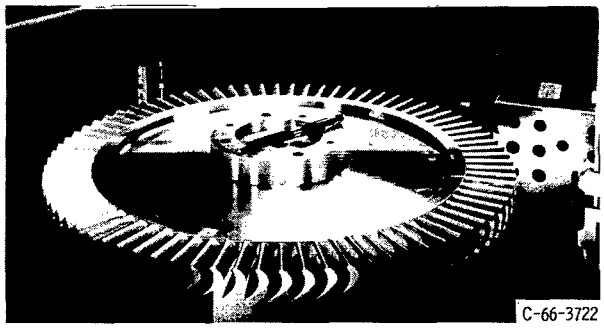

(b) Second-stage rotor without tip shroud.

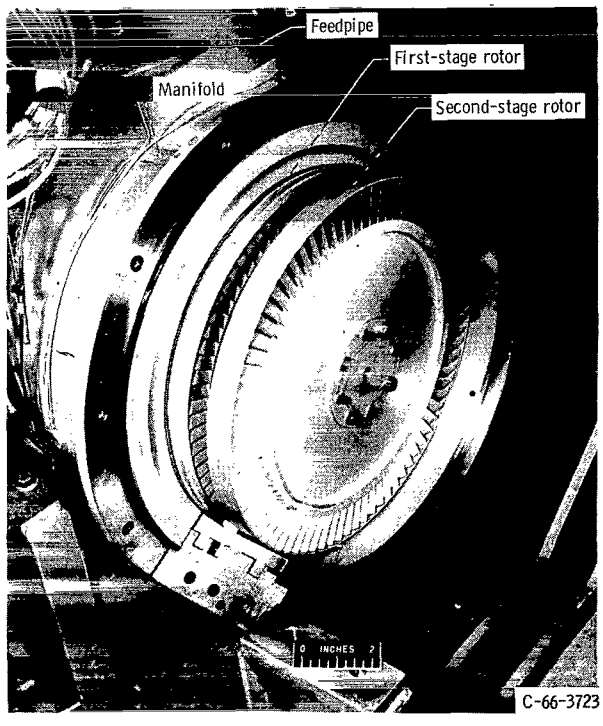

(c) Turbine assembly without half of casing.

Figure 6. - Scale-model turbine.

rotor removed and stator replaced by a fixture having similar inner and outer walls) were also tested.

APPARATUS

The test facility described in references 2 and 3 was used for this investigation. A diagram and overall view of the facility with the test turbine installed is shown in figures 7(a) and (b), respectively.

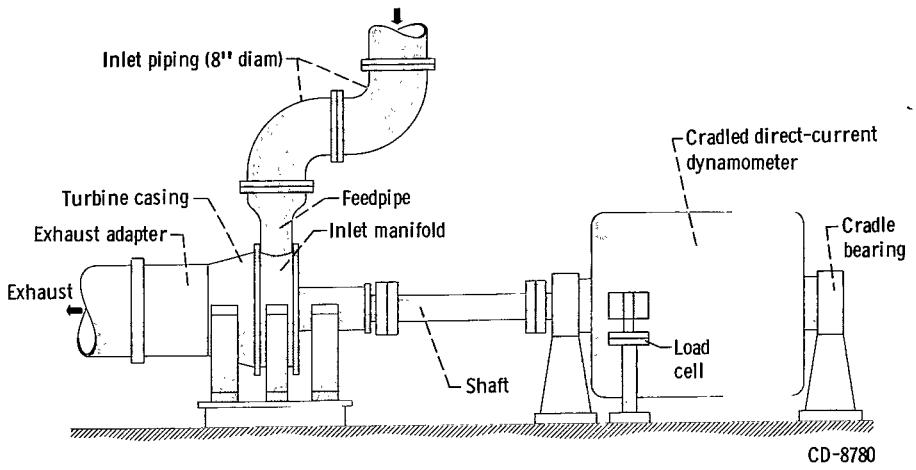

(a) Schematic diagram.

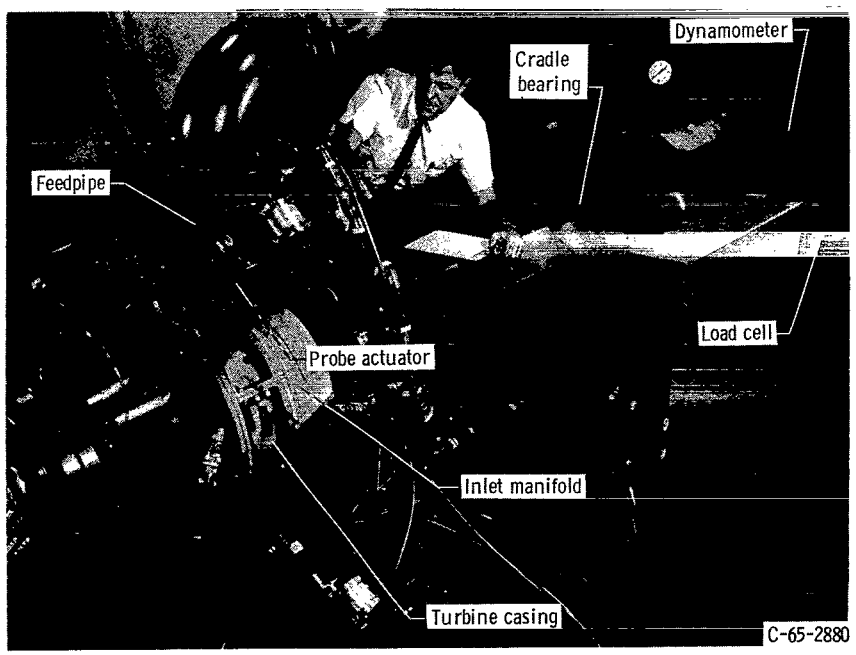

(b) Turbine installation.

Figure 7. - Turbine test facility.

In operation, compressed dry air from the laboratory supply flows through an electric heater, a calibrated orifice run, a pressure control valve, two 8-inch-diameter 90° elbows, and a reducer to the manifold feedpipe. After passing through the turbine, the air is discharged through an exhaust pressure control valve to the laboratory altitude exhaust system. Turbine output power was absorbed by a cradled direct-current electric dynamometer, which also served as the speed controller.

INSTRUMENTATION

The axial and circumferential location of instrumentation in the test turbine is shown in figure 8. Stations 3 and 5 are located 1/16 inch axially upstream from the blade trailing edge; station 4 is 1/16 inch axially downstream from the blade leading edge. The total pressure probe at station 6 was shielded to decrease angle sensitivity and was set at the design flow angle at the blade mean radius.

In addition to the fixed instrumentation, two combination total pressure - temperature - flow angle survey probes and one wedge type static pressure survey probe were located one blade chord downstream of the second rotor exit (station 6).

For tests of the first-stage configuration, the three survey probes and the fixed total pressure probe were located one blade chord downstream of the first-stage rotor. Figure 9 is a view of the rotor exit showing the stator wall simulation fixture and the survey instrumentation.

For tests of the feedpipe-manifold-nozzle configuration, a total pressure survey probe was located 1/8 inch downstream from the nozzle exit. The probe was shielded and was set at the design flow angle. Figure 10 is a view of the nozzle exit showing the probe and the survey equipment, which were also used for the oxidizer turbine tests (ref. 2).

The free stream probes used in this investigation are shown in figure 11. The angle sensing probes were flow calibrated to determine heading at balance, and they were installed to a radial position error less than 0.010 inch and an angle error less than 1°.

Air flow rate was measured with a calibrated ASME thin plate orifice. Orifice inlet pressure was measured with a calibrated precision Bourdon tube gage. All other pressures were recorded simultaneously by photographing a bank of mercury manometers.

Temperatures were read from an industrial self-balancing indicating potentiometer. Turbine rotative speed was measured with an electronic counter in conjunction with a magnetic pickup and a 60-tooth shaft-mounted gear.

Torque was converted to pressure by a self-balancing pneumatic load cell that was calibrated in place before and after each day's operation by deadweight loading the dynamometer stator.

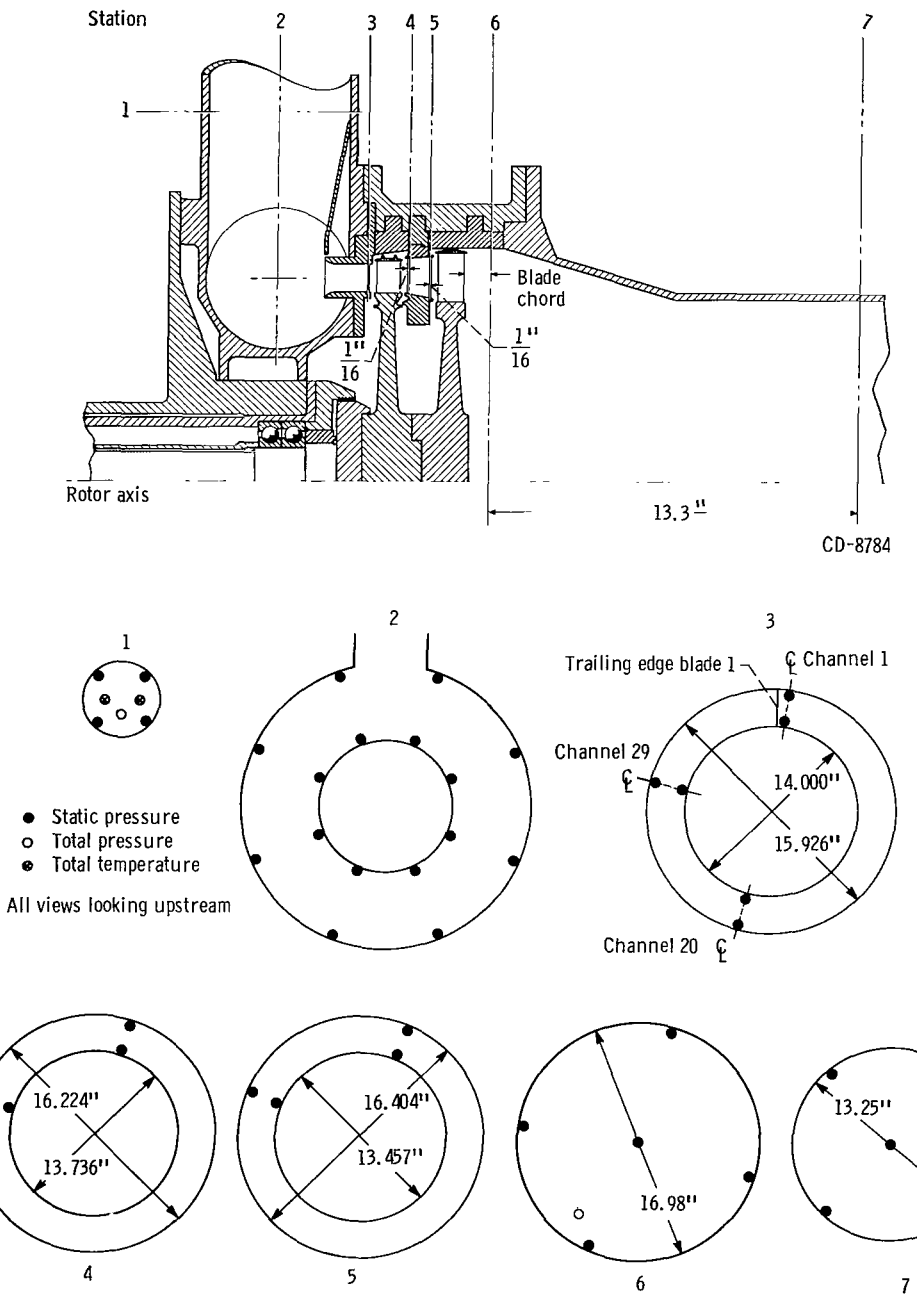

Figure 8. - Instrumentation location in scale-model turbine.

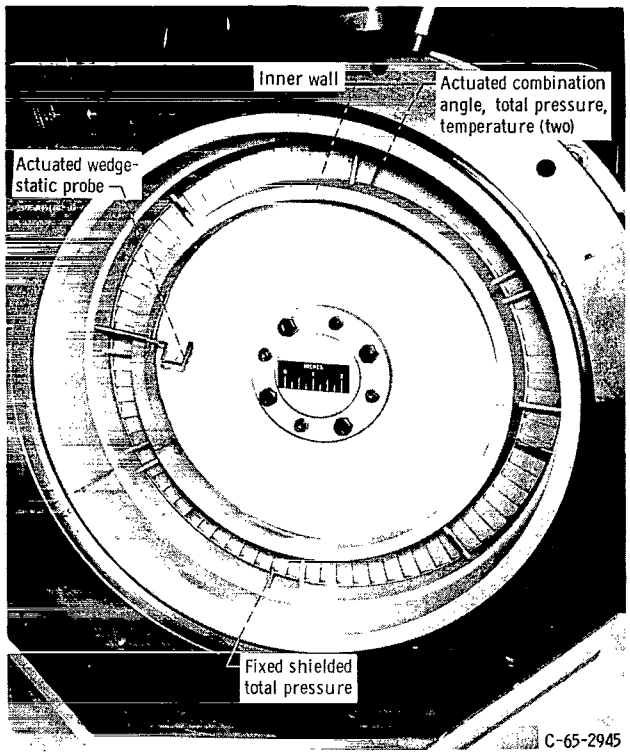

Figure 9. - Rotor exit instrumentation for first-state test.

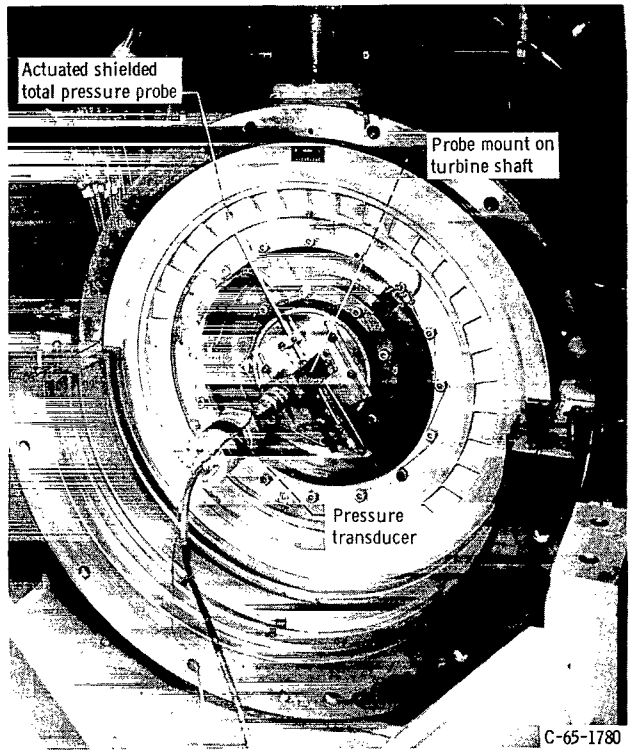

Figure 10. - Instrumentation for feedpipe-manifold-nozzle tests.

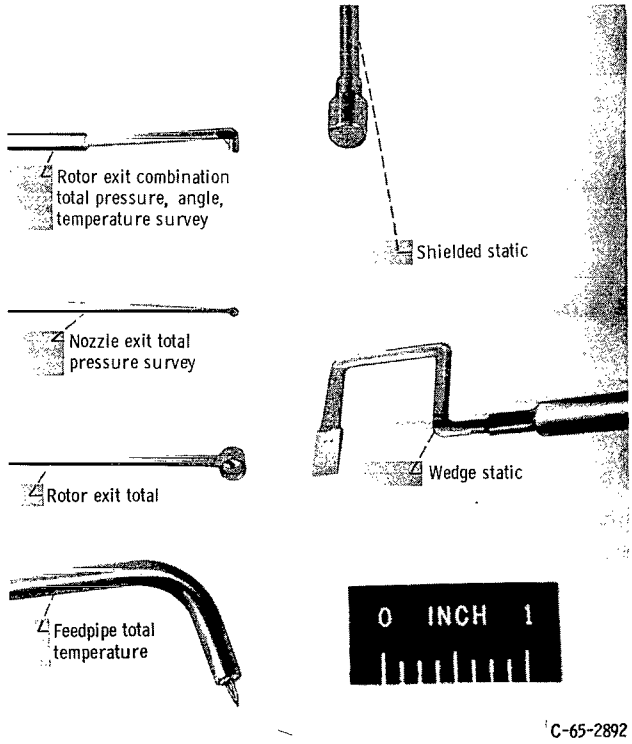

Figure 11. - Pressure and temperature probes.

PROCEDURE

Inlet total conditions for all tests were dry air at 25 psia and 600° R. The feedpipe-manifold-nozzle assembly was tested over a range of inlet total to nozzle exit static pressure ratios of 1.2 to 2.7. Higher pressure ratios could not be reached because of the flow limitations imposed by the large amount of whirl at the nozzle exit. Circumferential total pressure surveys were made at three radial positions at each pressure ratio. Pressure and probe position were recorded continuously. This procedure is described in detail in reference 2.

The two-stage test turbine was operated at 60, 80, 90, 100, and 105 percent of design equivalent speed at several inlet total to exit static pressure ratios. Weight-flow, torque, pressure, and temperature data were recorded at each pressure ratio and speed during steady-state operation. Zero-speed torque data were taken over a range of pressure ratios from 1.5 to 6.0. The same procedure was used for tests on the first stage. Performance data were taken over a range of pressure ratios from 1.5 to 5.0 and zero-speed torque data over a range of pressure ratios from 1.25 to 3.5.

First- and second-stage rotor exit flow conditions were surveyed at design equivalent speed and pressure ratio. Total pressure, total temperature, and flow angle were determined at several points along the blade span at two circumferential locations. Rotor exit static pressures were measured at several points between the outer wall and the turbine axis.

The turbine specific work was calculated from weight-flow, speed, and torque measurements. The torque value used was the sum of the torque indicated by the pneumatic load cell and the test unit bearing and seal torque.

The test unit bearing and seal torque was measured by motoring the test unit, with the rotors removed, over the range of speed investigated. This torque was approximately 1 percent of the two-stage turbine design torque.

The inlet or feedpipe total pressure was calculated from the average static pressure in the feedpipe, the flow area, the average inlet total temperature, and the weight flow in the same manner as in reference 2.

Interstage static pressures at the hub or tip sections were computed by averaging the pressures obtained from the hub or tip static taps at a given station (see fig. 8). Exit static pressures such as $\overline{p}_{3,m}$ and $\overline{p}_{4,m}$ were computed by averaging the hub and tip static pressures at stations 3 and 4, respectively. The two-stage turbine performance is based on the pressure ratio determined by the calculated inlet total pressure and the average static pressure at station 7 in the exhaust adapter $p_1'/\overline{p}_7$. First-stage performance is based on the pressure ratio $p_1'/\overline{p}_{4,m}$. All pressure ratios are equivalent values for air ($\gamma = 1.4$); these may be corrected for gases having different ratios of specific heats by the method given in reference 2.

RESULTS AND DISCUSSION

The results of the cold-air performance evaluation of the scale-model fuel turbine are presented in the following sections: Feedpipe-Manifold-Nozzle Assembly, First-Stage Performance, and Two-Stage Performance. The first- and two-stage turbine tests were performed with the inlet manifold assembly in place and the performance data presented includes losses attributable to the inlet manifold assembly.

Feedpipe-Manifold-Nozzle Assembly

The feedpipe-manifold-nozzle assembly was investigated over a range of inlet total to nozzle exit static pressure ratios ($p_1'/\bar{p}_{3,m}$) from approximately 1.2 to 2.7. The design pressure ratio of 4.221 could not be reached because of the flow limitations caused by the large amount of whirl at the nozzle exit.

Weight flow. - Equivalent weight flow as a function of inlet total to nozzle exit static pressure ratio is shown in figure 12. The nozzle chokes at a pressure ratio of approximately 1.5 and the equivalent weight flow is constant beyond this point. The actual equivalent weight flow is 2.88 pounds per second, which is 1.5 percent greater than the design value of 2.837 pounds per second. The equivalent flow was also constant at 2.88 pounds per second for inlet total to nozzle exit static pressure ratios greater than 1.5 for both first- and two-stage turbine tests. Therefore, weight flow will not be discussed in subsequent sections.

Feedpipe and manifold static pressures. - The static pressures in the feedpipe and manifold were constant for inlet total to nozzle exit static pressure ratios greater than 1.5 and were identical in value for all three of the test configurations. The static to total pressure in the feedpipe $\bar{p}_1/p_1'$ was 0.958, which indicates a feedpipe Mach number of 0.249.

The circumferential distribution of the manifold inner and outer wall static to inlet total pressure ratios p_2/p_1' at an inlet total to nozzle exit static pressure ratio of 1.51 is shown in figure 13. The lack of symmetry of static pressure about the feedpipe centerline is an indication of correspondingly asymmetrical flow conditions within the manifold. The lowest static pressures occur at the static taps adjacent to the feedpipe, and the inner and outer wall static pressures are reversed. This is the result of the flow turning from the radial to the tangential direction as it enters the man-

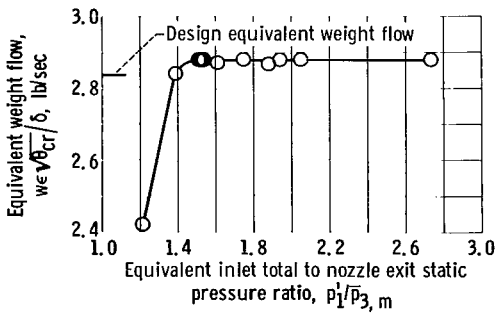

Figure 12. - Variation of equivalent weight flow with pressure ratio.

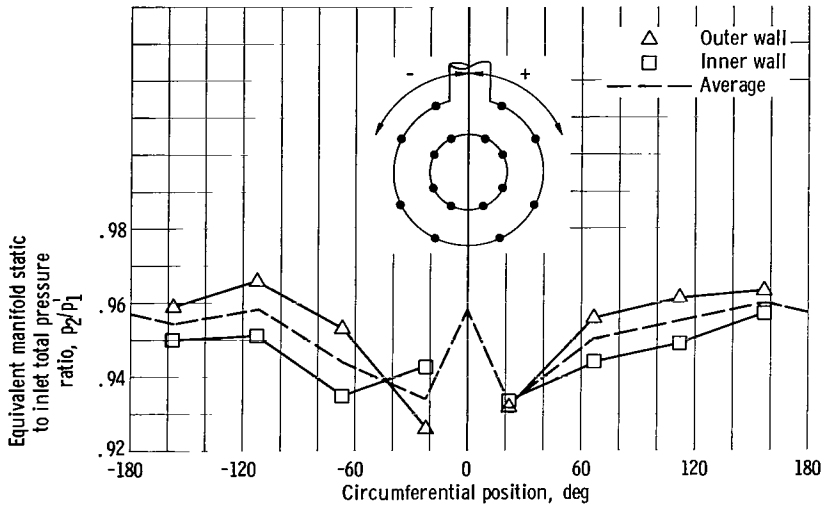

Figure 13. - Manifold circumferential static pressure distribution at inlet total to nozzle exit static pressure ratio of 1.51.

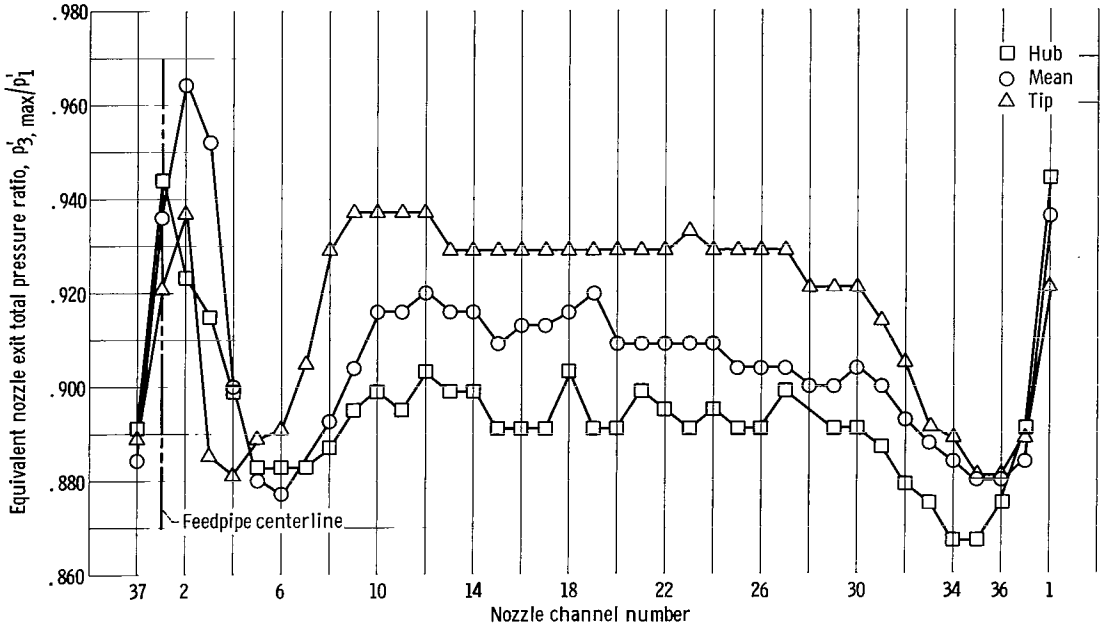

Figure 14. - Nozzle exit circumferential total pressure distribution at inlet total to nozzle exit static pressure ratio of 1.51.

ifold from the feedpipe. The acceleration of the flow and the attendant high local velocities result in the low static pressures. The average value of manifold static to inlet total pressure ratio $\bar{p}_{2,\,m}/p_1$ was 0.949. The design value was 0.98.

Nozzle exit total pressure surveys. - The results of hub, mean, and tip section nozzle exit total pressure surveys at an inlet total to nozzle exit static pressure ratio of 1.51 are shown in figure 14. The ratio of the maximum total pressure recorded for each nozzle channel to the inlet total pressure ($p'_{3,\,max}/p'_1$), is plotted against channel number (see fig. 8, p. 14). Large variations in nozzle exit total pressure are confined to approximately one-third of the nozzle circumference centered about the feedpipe. The maximum circumferential variation in nozzle exit total pressure is approximately 11 percent of inlet total pressure. The highest pressures occurred at the three channels opposite the feedpipe and the lowest at the five channels either side of and adjacent to the feedpipe. These low pressures are caused by incidence losses at the channel inlet resulting from the comparitively high local tangential velocities discussed previously. The effects of this incidence persist into the nozzle channel and cause further losses on the suction surface side of the channel. These losses were more pronounced for channels on the left side of the manifold (looking upstream) where flow incidence at the channel inlet was positive. The losses due to incidence effects, however, were less severe than those reported in reference 2 for the oxidizer turbine feedpipe-manifold-nozzle assembly where the tangential velocities in the manifold were higher than they are for the fuel turbine.

The average of the nozzle exit maximum total pressures, obtained from the mean diameter data of figure 14 are plotted against inlet total to nozzle exit static pressure ratio in figure 15. The nozzle exit total pressure first decreases, then increases with increasing overall pressure ratio. Reference 6 indicates this to be characteristic of convergent-divergent nozzles operated at off-design pressure ratios. The flow in convergent-divergent nozzles overexpands - reaching sonic velocity at the throat at overall pressure ratios less than critical (critical flow occurred in the feedpipe-manifold-nozzle assembly at an overall pressure ratio of only 1.5). As the nozzle exit static pressure is decreased, shock and diffusion in the divergent portion of the nozzle channel then cause total pressure losses which first increase and then decrease, reaching a minimum when the flow in the divergent section is fully expanded. The maximum nozzle exit total pressures, then, cannot be considered to be equal to the effective nozzle inlet total pressure as was done in reference 2. The circumferential variation of total pressure at the nozzle inlet, however, would probably have the same characteristics as shown in figure 14, but with a higher average total pressure.

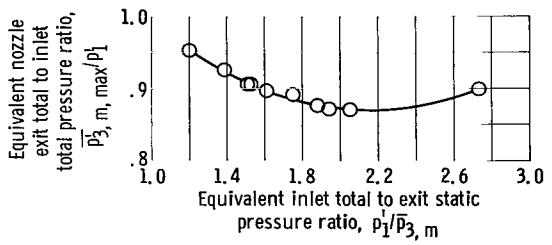

Figure 15. - Variation of nozzle exit total pressure with nozzle pressure ratio.

Design inlet total to nozzle exit static pres-

sure ratio could not be reached, as previously discussed; therefore, the loss in total pressure between the feedpipe and the nozzle inlet ($p_1' - \overline{p}_2'$) could not be determined experimentally. The ratio $\overline{p}_2'/p_1'$ was calculated from continuity and the procedure of reference 4 and was found to be 0.950. This approximates the loss of 1.2 inlet velocity heads. The design value of $\overline{p}_2'/p_1'$ was 0.98.

First-Stage Performance

The first-stage rotor testing was performed with the feedpipe-manifold-nozzle assembly in place. The second-stage stator was replaced by a fixture having inner and outer walls similar to those of the stator. The performance investigation covered a range of equivalent inlet total to first-stage rotor exit static pressure ratios ($p_1'/\overline{p}_{4,\,m}$) of approximately 1.5 to 5.0, each at constant equivalent speeds of 60, 80, 90, 100, and 105 percent of design.

Equivalent specific work. - Equivalent specific work as a function of equivalent inlet total to exit static pressure ratio and percent equivalent speed is shown in figure 16. The actual equivalent specific work at design equivalent speed and pressure ratio is 21.3 Btu per pound, which is 3.5 percent greater than the design value of 20.566 Btu per pound. The shallow slope of the equivalent specific work curves at the higher pressure ratios

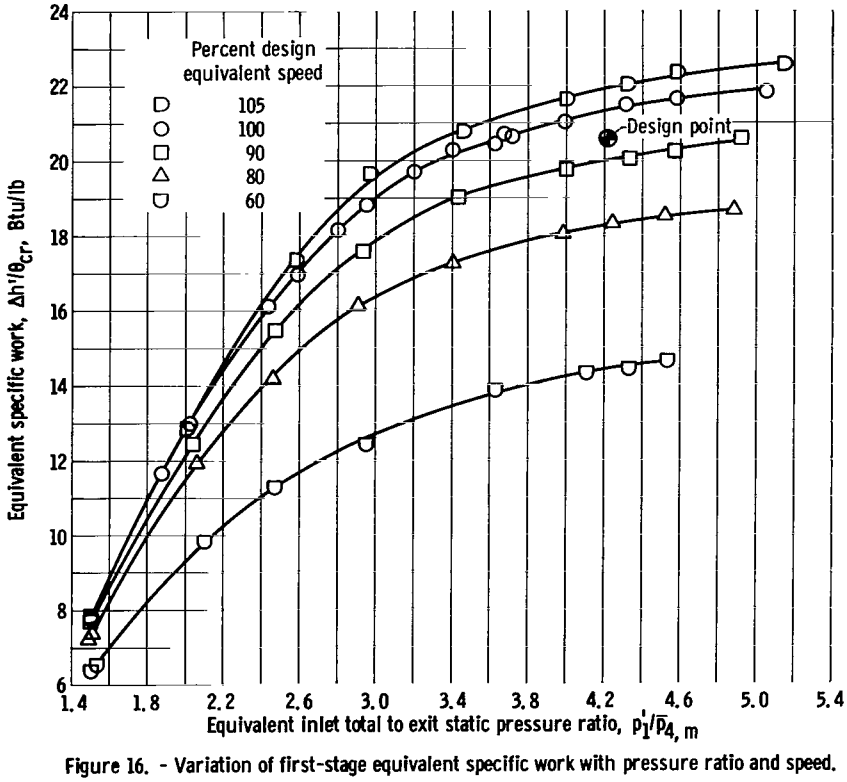

Figure 16. - Variation of first-stage equivalent specific work with pressure ratio and speed.

indicates that the first stage was approaching limiting loading.

Equivalent torque. - Equivalent torque as a function of percent equivalent speed and overall pressure ratio is shown in figure 17. Zero-speed torque could not be obtained for pressure ratios greater than 3.5 because of the excessive whirl at the rotor exit. The torque curves were extrapolated to zero speed for pressure ratios greater than 3.5. The equivalent torque at design equivalent speed and pressure ratio is 104 pound-feet, which is 3.6 percent greater than the design value of 99.47 pound-feet. At first-stage design equivalent inlet total to exit static pressure ratio, the ratio of zero speed to design speed equivalent torque is approximately 1.31.

Static efficiency. - Static efficiency as a function of blade-jet speed ratio and percent design equivalent speed is shown in figure 18. At the first-stage-design blade-jet speed ratio of 0.196 and design equivalent speed, the static efficiency is 0.51 compared to 0.490 design. The maximum static efficiency attained was approximately 0.59 at a blade-jet speed ratio of 0.247 and 105-percent design equivalent speed. The static efficiency does not continue to increase as expected at the higher blade-jet speed ratios; instead, the efficiency falls off and the constant speed lines seem to be converging. This effect is also evident in figure 17. At low pressure ratios corresponding to high blade-jet speed ratios, there is only a small, and decreasing,

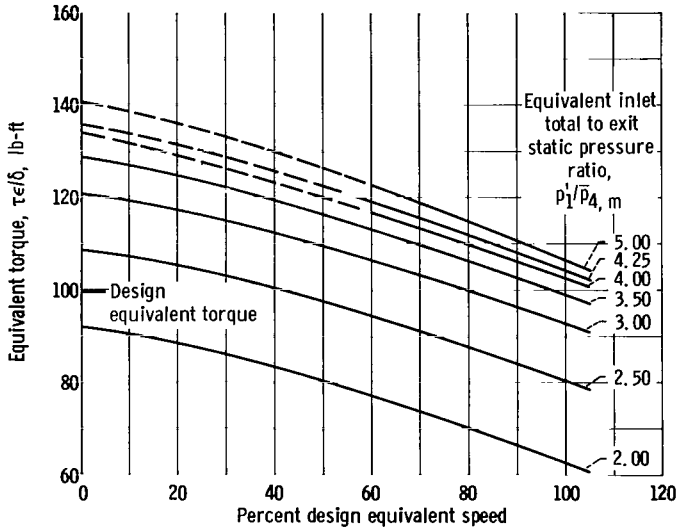

Figure 17. - Variation of first-stage equivalent torque with speed and pressure ratio.

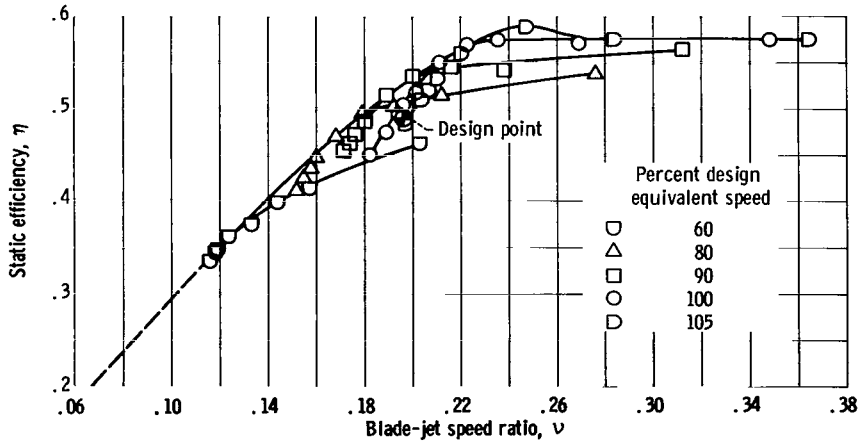

Figure 18. - Variation of first-stage static efficiency with blade-jet speed ratio and speed.

change in equivalent specific work with speed. This is probably due to the decrease in nozzle efficiency at low pressure ratios which was discussed in the nozzle exit total pressure survey section. The rapid decrease in static efficiency at constant speed and low blade-jet speed ratio is due to first-stage operation close to limiting loading at the high overall pressure ratios corresponding to low blade-jet speed ratios.

First-stage rotor exit surveys. - Radial surveys of first-stage rotor exit flow conditions were taken at design equivalent speed and nominally design inlet total to exit static pressure ratio. Absolute flow angle, total pressure, and total temperature were measured with two actuated combination probes at several radial locations along the blade span. These measurements were made at a station one blade chord downstream of the rotor trailing edge. Static pressure measurements were made from the outer wall to the shaft centerline. The procedures and instruments used have been described in their respective sections.

The radial variation of first-stage rotor exit flow angle is shown in figure 19. There

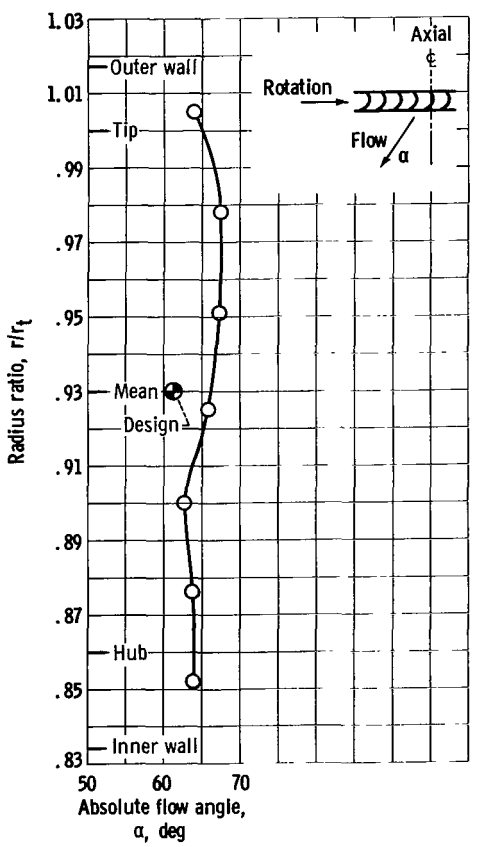

Figure 19. - Radial variation of first-stage rotor exit flow angle at design equivalent pressure ratio and speed.

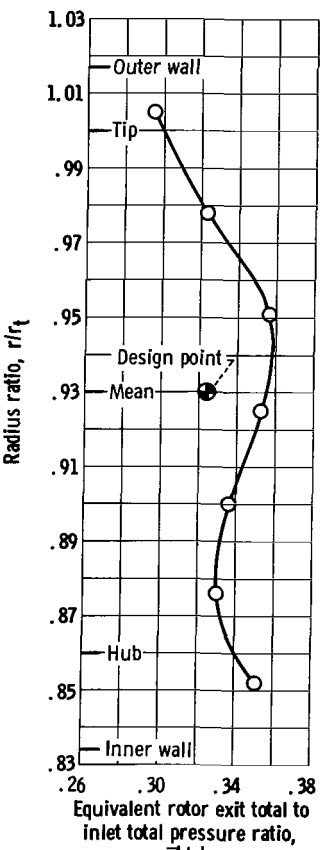

Figure 20. - Radial variation of first-stage rotor exit total pressure at design equivalent pressure ratio and speed.

is comparatively little variation in angle across the blade span. The average angle is 65° from axial compared to 61.25° design. The rotor exit area was 3.1 percent less than design. This smaller area would contribute to the observed overturning of the flow. The radial variation of first-stage rotor exit to inlet total pressure ratio $\overline{p}_4'/p_1'$ is shown in figure 20. The trend of the first-stage rotor exit total pressure is similar to that of the flow angle (see fig. 19), but there is more variation across the blade span. The minimum value of rotor exit to inlet total pressure ratio of 0.295 occurs near the tip section, and the maximum ratio of 0.358 occurs near the mean diameter. The average value is 0.335 compared to 0.324 design. First-stage local total efficiency, computed from the total temperature and total pressure survey data, is shown in figure 21. There is a pronounced variation in total efficiency across the blade span. The shape of this curve is, however, similar to those of flow angle and total pressure (figs. 19 and 20). The maximum local total efficiency of 0.71 occurs near the mean diameter and falls off rapidly to a minimum of 0.51 near the tip section. The average value of first-stage total efficiency is 0.64

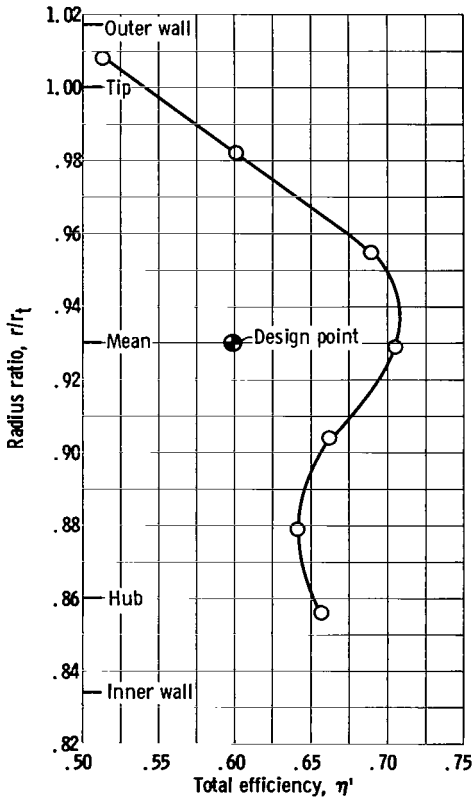

Figure 21. - Radial variation of first-stage rotor total efficiency at design equivalent pressure ratio and speed.

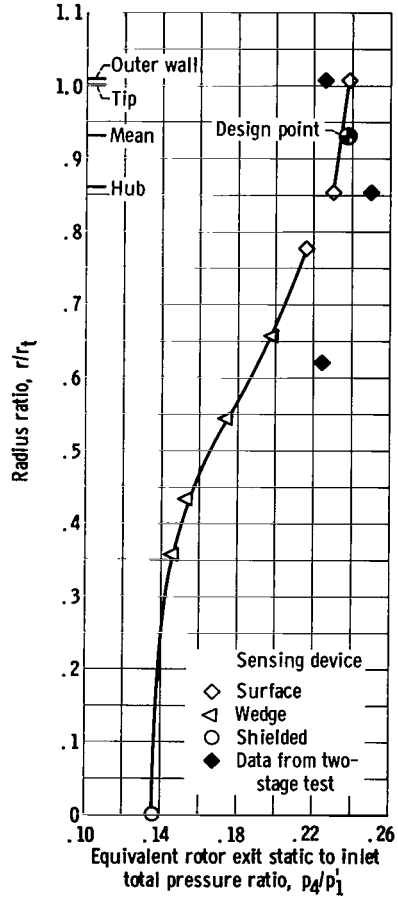

Figure 22. - Radial variation of first-stage rotor exit static pressure at design equivalent pressure ratio and speed.

compared to 0. 599 design.

Static pressure data for the region from the turbine shaft centerline to the outer wall are shown in figure 22. The type of sensing element used for each data point is indicated on the figure. There is a fairly large radial static pressure gradient along the first-stage rotor face from the shaft centerline to the outer wall. This is probably due to the large amount of whirl at the first-stage rotor exit (see velocity diagrams, fig. 3, p. 6). The pressure gradient across the blade span is small and positive from hub to tip walls. Second-stage stator tip, hub, and diaphragm static pressure data from the two-stage tests at design point operation are also shown on figure 22. The addition of the second-stage rotor and stator did have an effect on the first-stage rotor radial exit static pressure distribution. This is discussed further under Two-Stage Turbine Performance in the Interstage static pressures section.

Two-Stage Turbine Performance

The two-stage turbine test configuration was as shown in figure 8 (p. 14). The investigation covered a range of equivalent inlet total to exit static pressure ratios $p_1'/\bar{p}_7$ from approximately 1. 5 to 6. 0 each at constant speeds of 60, 80, 90, 100, and 105 percent design equivalent speed.

Equivalent specific work. - Two-stage turbine equivalent specific work as a function of inlet total to exit static pressure ratio and percent design equivalent speed is shown in figure 23. At design equivalent speed and pressure ratio the equivalent specific work was 29. 7 Btu per pound, which is 4. 5 percent greater than the design value of 28. 428 Btu per pound. The first-stage equivalent specific work was 21. 3 Btu per pound or 71. 7 percent of the total. The design value was 72. 3 percent.

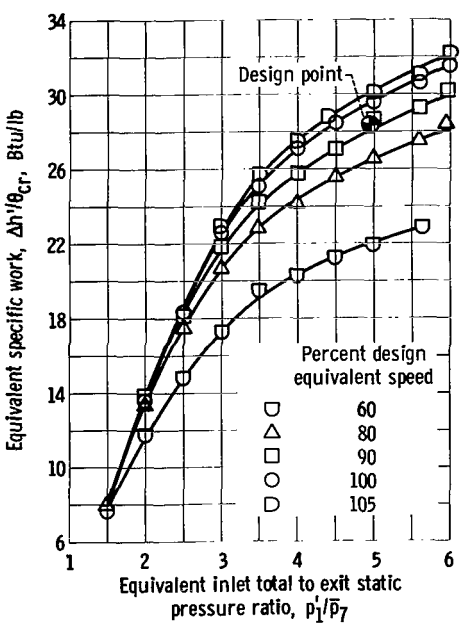

Figure 23. - Variation of two-stage equivalent specific work with pressure ratio and speed.

The two-stage turbine was not operating near limiting loading as evidenced by the continuing increase in equivalent specific work at the highest pressure ratios investigated. The constant speed lines become coincident at low overall pressure ratios. This occurs because the feedpipe-manifold total pressure loss (which is constant) and the exit leaving loss become larger proportions of the available enthalpy and also because the nozzle losses increase as the overall pressure ratio decreases.

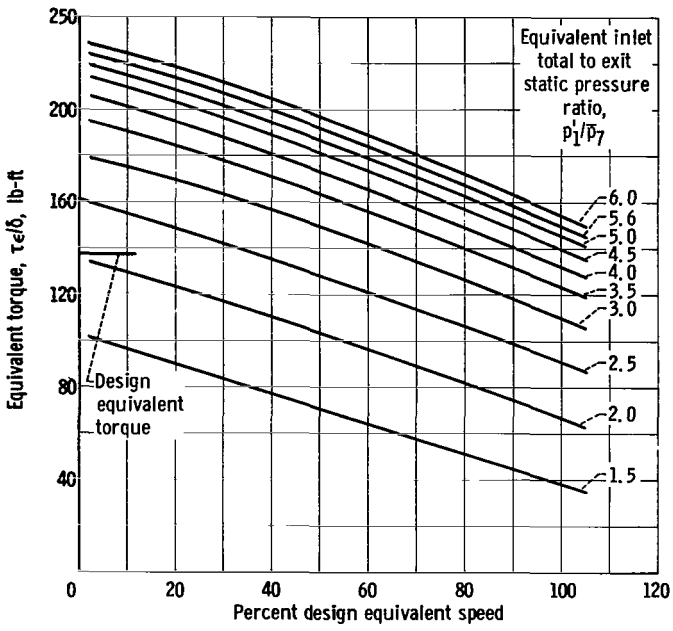

Figure 24. - Variation of two-stage turbine equivalent torque with pressure ratio and speed.

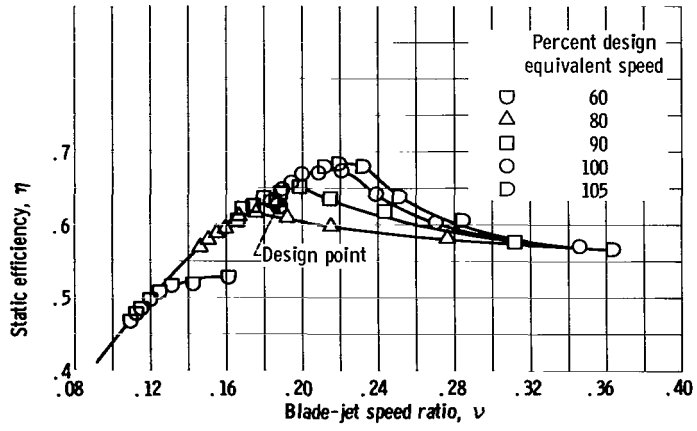

Figure 25. - Variation of two-stage static efficiency with blade-jet speed ratio and speed.

Equivalent torque. - Figure 24 shows equivalent torque as a function of percent design equivalent speed and equivalent inlet total to exit static pressure ratio. At design equivalent speed and approximately design equivalent pressure ratio of 5.0, the actual equivalent torque is 145 pound-feet, which is 4.8 percent greater than the design value of 137.41 pound-feet. The ratio of zero to design speed torque at the design pressure ratio is 1.52.

Static efficiency. - The two-stage turbine static efficiency as a function of blade-jet speed ratio and percent design equivalent speed is shown in figure 25. At design equivalent speed and blade-jet speed ratio of 0.188, the actual static efficiency is 0.65 compared to 0.622 design. Maximum static efficiency of 0.685 occurred at a blade-jet speed ratio of 0.224 and 105-percent design equivalent speed. The two-stage turbine does not operate as close to the limiting loading condition as did the first stage, and the constant speed lines merge with the efficiency envelope as the blade-jet speed ratio decreases rather than falling off rapidly as was the case with the first stage (fig. 18, p. 21). The 80, 90, 100, and 105 percent design equivalent speed lines level off and converge at the higher blade-jet speed ratios. This is a result of the coincidence of the corresponding lines at low overall pressure ratios noted in the discussion of equivalent

specific work (fig. 23, p. 24).

Second-stage rotor exit surveys. - Radial surveys of the second-stage rotor exit flow conditions were made at station 6 (fig. 8, p. 14). The procedure and instruments used were the same as those described in the First-stage rotor exit survey section.

The second-stage rotor exit flow angle (fig. 26) shows considerably more radial variation than the first-stage exit angle (fig. 19, p. 22). There is appreciable overturning of the flow over much of the blade span. The flow at the tip section, however, is very much underturned. This may have been caused by leakage flow around the rotor tip shroud. At the mean diameter, the measured angle was 33° from axial, and the average angle is 29.9° compared to 27.1° design. The rotor exit area was 1.57 percent less than design which would result in some overturning of the flow.

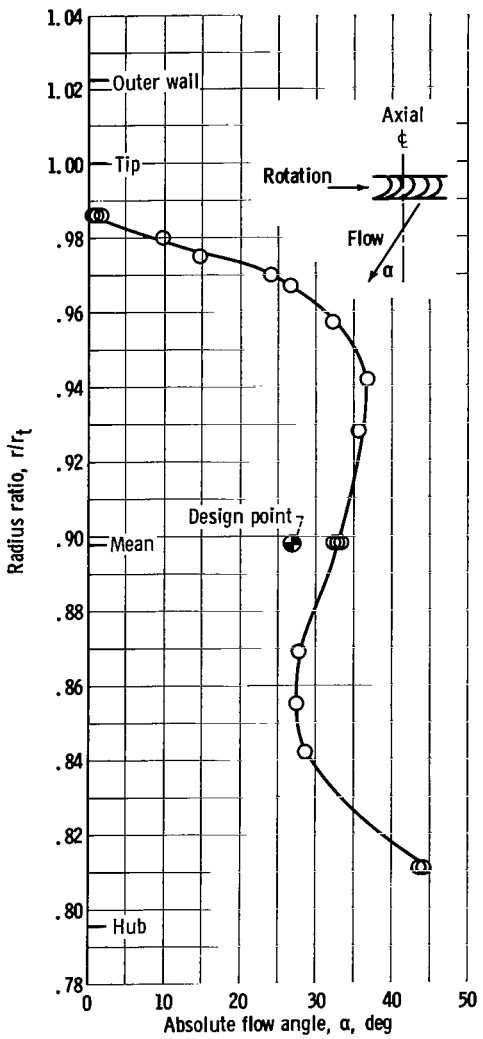

Figure 26. - Radial variation of second-stage rotor exit flow angle at design equivalent pressure ratio and speed.

The radial variation of the second-stage rotor exit to inlet total pressure ratio $\bar{p}_6'/p_1'$ is shown in figure 27. There is very little radial variation, and the average value of $\bar{p}_6'/p_1'$ is 0.214 compared to 0.212 design. The minimum value of 0.211 occurred at the tip section.

Local total efficiency, computed from the second-stage rotor exit total temperature and pressure survey data, is shown in figure 28. There is considerable radial variation in the total efficiency. The maximum value of 0.695 occurs at the mean diameter and the minimum value of 0.605 occurs at the tip section. The average value of two-stage turbine total efficiency is 0.67 compared to the design value of 0.640.

The second-stage rotor exit static to inlet total pressure ratio p_6/p_1' is shown in figure 29. The radial static pressure gradient is quite small from the shaft centerline to the blade hub section and very small across the blade span. The whirl at the second-stage rotor exit is much smaller than that of the first-stage and, therefore, the radial static pressure gradient is also less.

Interstage static pressures. - The location of the axial stations and wall static taps are shown in figure 8 (p. 14). Hub and tip static pressure taps were provided for all blade rows except the second-stage rotor exit (station 6) and for the exhaust pipe

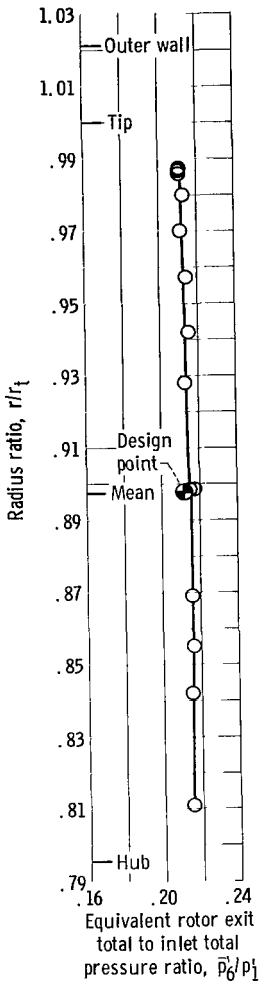

Figure 27. - Radial variation of second-stage rotor exit total pressure at design equivalent pressure ratio and speed.

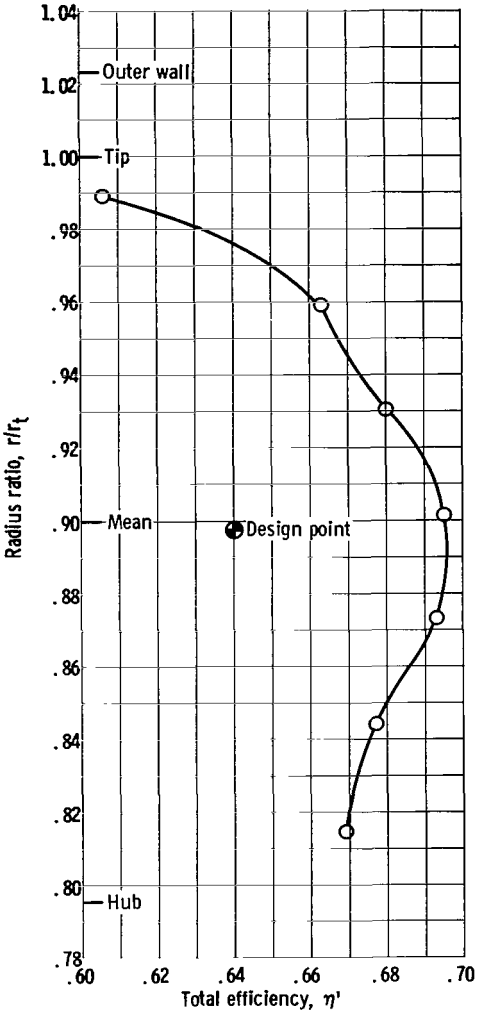

Figure 28. - Radial variation of two-stage turbine total efficiency at design equivalent pressure ratio and speed.

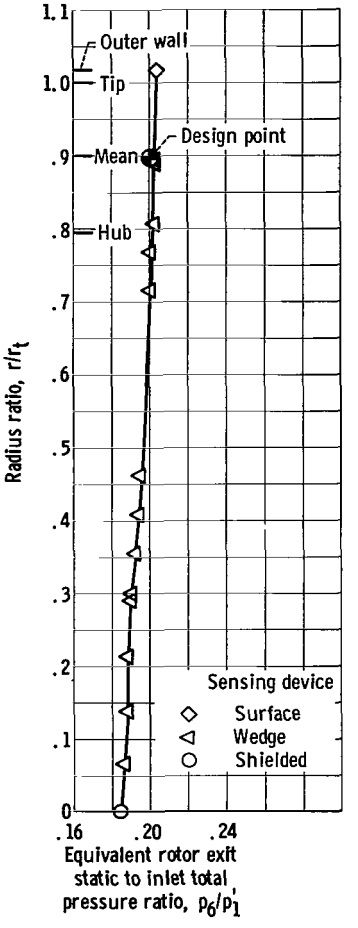

Figure 29. - Radial variation of second-stage rotor exit static pressure at design equivalent pressure ratio and speed.

(station 7) where only tip or outer wall taps could be provided.

The average nozzle hub and tip exit static to inlet total pressure ratios for both two- and first-stage turbine configurations and at design equivalent speed are shown as functions of the equivalent inlet total to first-stage exit static pressure ratio $p_1'/\bar{p}_{4,m}$ in figure 30. There is comparitively little change in the nozzle exit static pressures as the overall pressure ratio increases from 4.0 to 6.0. This is an indication that the first-stage rotor is choking and preventing further decrease in nozzle exit static pressure. The design nozzle exit static to inlet total pressure ratio of 0.237 was never reached. At two-stage and first-stage design equivalent speed and pressure ratio, the nozzle exit

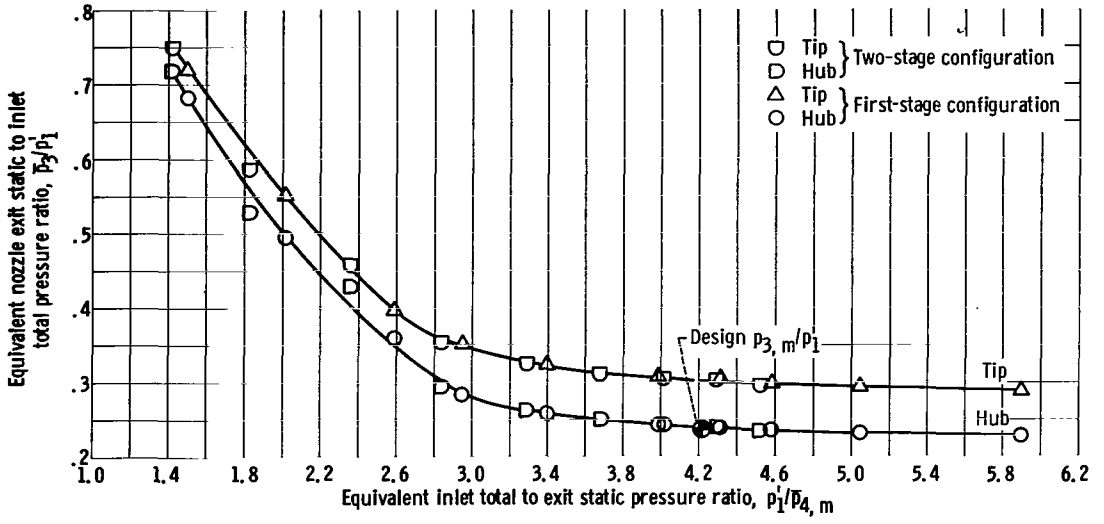

Figure 30. - Variation of nozzle exit static pressure with first-stage pressure ratio at design speed.

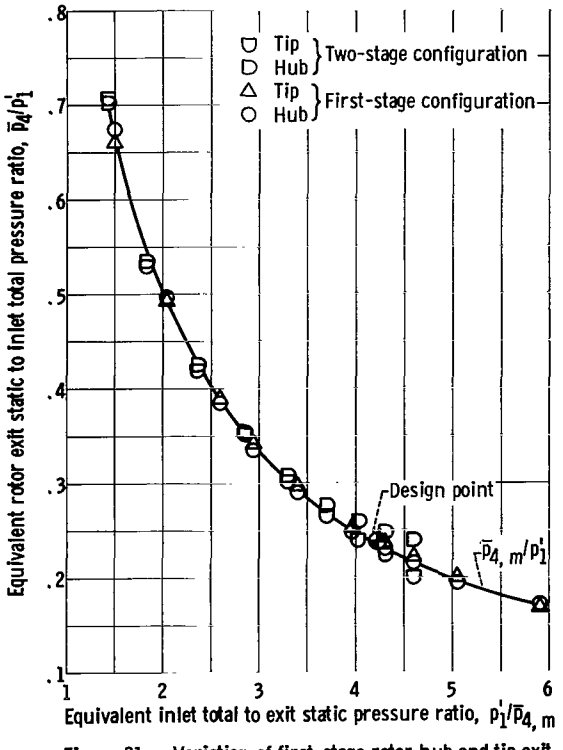

Figure 31. - Variation of first-stage rotor hub and tip exit static pressure with pressure ratio at design speed.

static to inlet total pressure ratio $\bar{p}_{3,m}/p_1'$ was 0.270. This would result in higher than design nozzle loss, as discussed in the Nozzle exit total pressure survey section, and less than design nozzle exit velocity.

The average first-stage rotor hub and tip exit static to inlet total pressure ratios for both first- and two-stage turbine configurations and at design equivalent speed are shown as functions of the equivalent inlet total to first-stage exit static pressure ratio $p_1'/\bar{p}_{4,m}$ in figure 31. At two-stage turbine design equivalent speed and pressure ratio, the inlet total to first-stage exit static pressure ratio $p_1'/\bar{p}_{4,m}$ was 4.25 compared to the design value of 4.221. Very little radial static pressure gradient is evident for the first-stage configuration over the range of pressure ratios investigated. The two-stage radial pressure gradient is also near zero but becomes increasingly negative (hub static pressure higher than tip static pressure) as the overall pressure ratio increases.

The axial distribution of tip and hub static pressure at several equivalent feedpipe total to exit static pressure ratios $p_1'/\bar{p}_7$ and at design

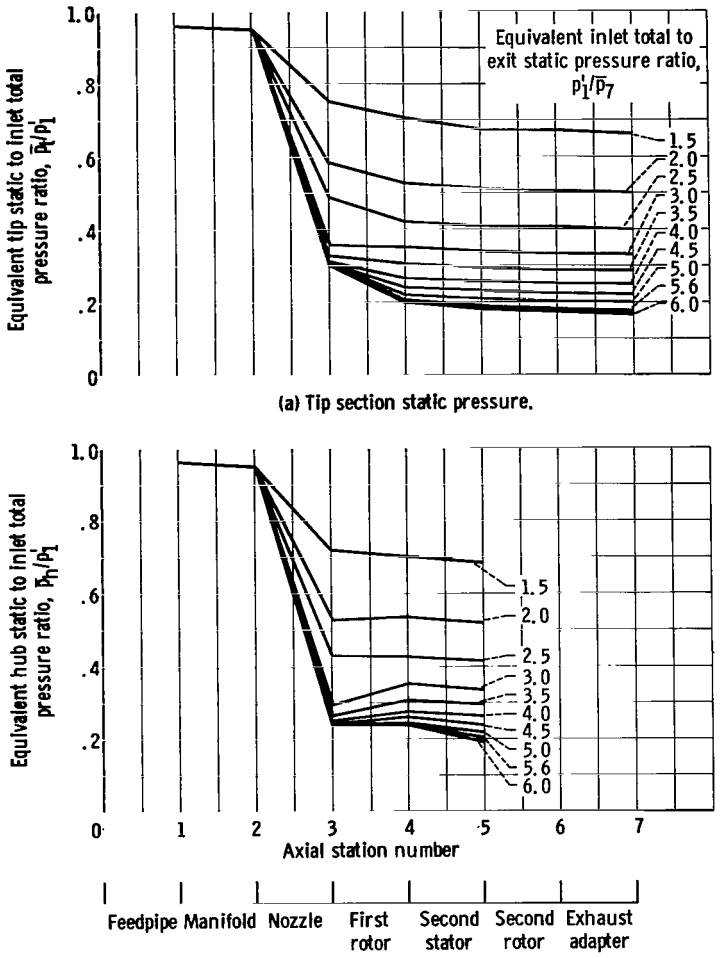

Figure 32. - Axial static pressure distribution at design equivalent speed.

equivalent speed are shown in figures 32(a) and (b), respectively. Almost all of the available pressure drop occurs in the nozzle. There are varying amounts of reaction across the first-stage rotor, positive at the tip section and negative at the hub section. At a pressure ratio near design (5. 0) there is almost no reaction at the first-stage rotor hub section and considerable positive reaction at the tip. This resulted in a near zero radial pressure gradient at the first-stage exit during the first-stage tests. The effect of the stator blades and the higher casing pressure (fig. 22) which occurred in the two-stage configuration apparently resulted in the negative radial static pressure gradient observed at station 4 (fig. 31).

Analysis of turbine performance. - Mean diameter blade speed, specific work, weight flow, static pressure, and the average values of flow angle and total pressure data were used to compute velocity diagrams representative of the turbine performance at design speed and pressure ratio. These are presented in figure 33. The axial distribution

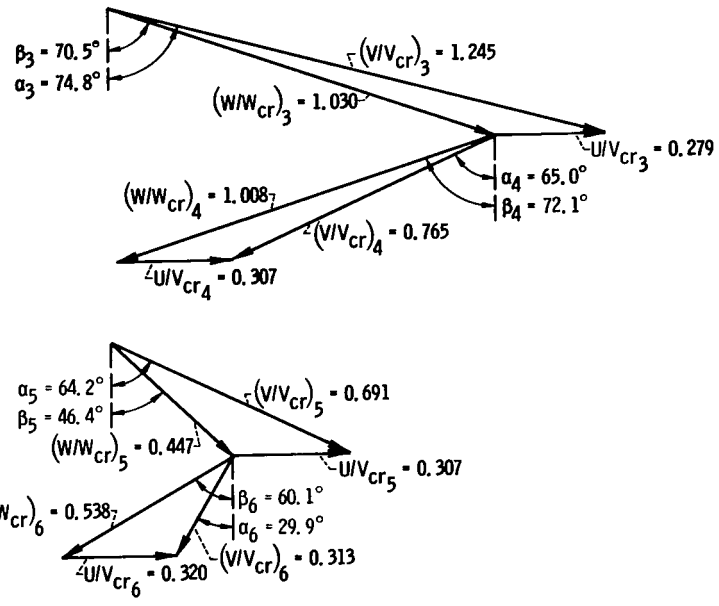

Figure 33. - Velocity diagrams obtained from experimental data at design equivalent pressure ratio and speed.

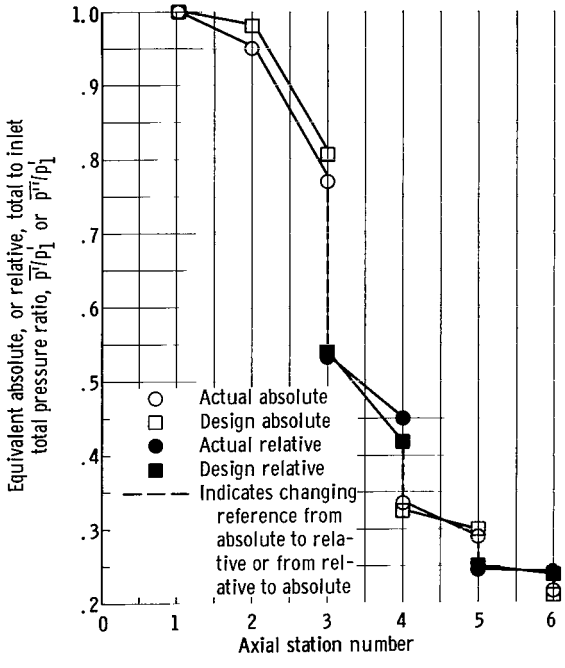

Figure 34. - Comparison of design and actual absolute and relative total pressures at design equivalent pressure ratio and speed.

of absolute and relative total pressure ratios corresponding to the velocity diagrams of figure 33 are shown in figure 34, where they are compared to the design values. The mean diameter actual and design axial static pressure distribution at design pressure ratio and speed are compared in figure 35.

An examination of these figures and a comparison of figure 33 with the design velocity diagrams (fig. 3, p. 6) indicates that the second stage was operating reasonably close to design. The most significant deviations from design performance occurred in the first stage. The first-stage rotor choked prematurely, a result of the 3.1-percent deficiency in rotor exit area, and prevented the nozzle from reaching design exit pressure. This, in turn, resulted in lower than design nozzle exit velocity, higher than design nozzle total pressure loss, and net positive reaction across the first-stage rotor (station 3 to 4, fig. 35) which had been designed to be a purely impulse row (no

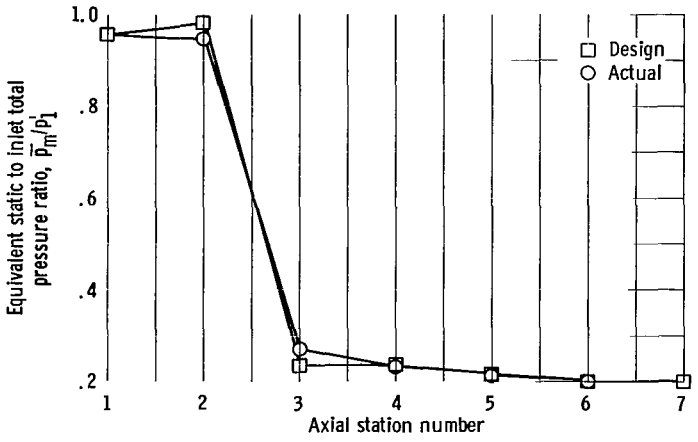

Figure 35. - Comparison of design and actual static pressures at mean diameter and at design equivalent pressure ratio and speed.

pressure change). The total pressure loss between the inlet station in the feedpipe and the nozzle exit (station 3) shown in figure 34 is larger than the design loss. This resulted from higher than design loss in the manifold, losses which occurred in the nozzle channels because of the poor flow conditions existing at the nozzle inlet (station 2) and the loss incurred when convergent-divergent nozzles are operated at less than design pressure ratio. These were discussed in the Feedpipe-Manifold-Nozzle Assembly section (p. 17).

The effect of the lower nozzle exit velocity in conjunction with positive reaction across the first-stage rotor is to decrease the relative velocity at the rotor inlet and increase the relative velocity to approximately critical at the rotor exit. The resultant diagram is an improvement over the design diagram as the work production is higher and the losses resulting from diffusion in the rotor are lower. The equivalent specific work of the first stage was 3.5 percent greater than design. The total pressure at the first-stage rotor exit was also higher than design in spite of the larger losses occurring in the feedpipe-manifold-nozzle assembly. This resulted from the lower than design loss in relative total pressure occurring in the first-stage rotor, as shown in figure 34. The first-stage total efficiency was 0.64; a four-point improvement over design.

SUMMARY OF RESULTS

The aerodynamic performance of a 0.646-scale-model fuel turbopump drive turbine for the M-1 rocket engine was determined experimentally. The turbine inlet manifold was first tested as a separate unit. Two-stage and first-stage configurations of the scale-model turbine, including the inlet manifold, were then tested over a range of speeds and pressure ratios. The results of these investigations can be summarized as follows:

1. Equivalent weight flow for all configurations was constant for inlet total to nozzle exit static pressure ratios greater than 1.5 where the nozzle choked. The actual equivalent weight flow was 2.88 pounds per second, which was 1.5 percent greater than design.

2. The circumferential variation in nozzle exit total pressure was largely confined to approximately one-third of the manifold centered in the feedpipe region. In this region the variation in nozzle exit total pressure was about 11 percent of inlet total pressure. A similar circumferential variation would exist at the nozzle inlet. Feedpipe-manifold total pressure losses could not be determined experimentally. This loss was calculated to be 5 percent of inlet total pressure, which approximates the loss of 1.2 inlet velocity heads.

3. At design equivalent speed and pressure ratio, the first-stage equivalent specific work was 21.3 Btu per pound and the static efficiency was 0.51. The design values were 20.566 and 0.490, respectively.

4. At design equivalent speed and pressure ratio, the two-stage turbine equivalent specific work was 29.7 Btu per pound and the static efficiency was 0.65. The design values were 28.428 and 0.622, respectively.

5. Radial surveys of rotor exit flow conditions indicated that the average values of flow angle, total pressure, and total efficiency were greater than design for both the first- and two-stage turbine configurations.

6. At design equivalent speed and pressure ratio, the inlet total to nozzle exit static pressure ratio was 3.7 compared to 4.22 design. All other mean diameter interstage static pressures were very near the design values and were substantially the same for all configurations.

7. Velocity diagrams constructed from the data indicated that the second stage was operating reasonably close to design and that first-stage operation deviated substantially from design. The net result, however, was an improvement in the first-stage velocity diagram and performance. First-stage total efficiency was 0.64 compared to 0.599 design.

Lewis Research Center,
National Aeronautics and Space Administration,
Cleveland, Ohio, September 23, 1966,
128-31-02-25-22.

REFERENCES

1. Beer, R.: Aerodynamic Design and Estimated Performance of a Two-Stage Curtis Turbine for the Liquid Oxygen Turbopump of the M-1 Engine. Rep. No. AGC-8800-12 (NASA CR-54764), Aerojet General Corp., 1965.

2. Stabe, Roy G.; Evans, David G.; and Roelke, Richard J.: Cold-Air Performance Evaluation of Scale Model Oxidizer Pump-Drive Turbine for the M-1 Hydrogen-Oxygen Rocket Engine. I - Inlet Feedpipe-Manifold Assembly. NASA TN D-3294, 1966.

3. Roelke, Richard J.; Stabe, Roy G.; and Evans, David G.: Cold-Air Performance Evaluation of Scale Model Oxidizer Pump-Drive Turbine for the M-1 Hydrogen-Oxygen Rocket Engine. II - Overall Two-Stage Performance. NASA TN D-3368, 1966.

4. Reynolds, T. W.: Aerodynamic Design - Model II Turbine M-1 Fuel Turbopump Assembly. Rep. No. AGC-8800-52 (NASA CR 54820), Aerojet General Corp., Apr. 15, 1966.

5. Holeski, D. E.; and Stewart, W. L.: Study of NASA and NACA Single-Stage Axial Flow Turbine Performance as Related to Reynolds Number and Geometry. J. Eng. Power, vol. 86, no. 3, July 1964, pp. 296-298.

6. Keenan, J. H.: Reaction Tests of Turbine Nozzles for Supersonic Velocities. ASME Trans., vol. 71, no. 7, Oct. 1949, pp. 773-780.

"The aeronautical and space activities of the United States shall be conducted so as to contribute . . . to the expansion of human knowledge of phenomena in the atmosphere and space. The Administration shall provide for the widest practicable and appropriate dissemination of information concerning its activities and the results thereof."

—NATIONAL AERONAUTICS AND SPACE ACT OF 1958

NASA SCIENTIFIC AND TECHNICAL PUBLICATIONS

TECHNICAL REPORTS: Scientific and technical information considered important, complete, and a lasting contribution to existing knowledge.

TECHNICAL NOTES: Information less broad in scope but nevertheless of importance as a contribution to existing knowledge.

TECHNICAL MEMORANDUMS: Information receiving limited distribution because of preliminary data, security classification, or other reasons.

CONTRACTOR REPORTS: Technical information generated in connection with a NASA contract or grant and released under NASA auspices.

TECHNICAL TRANSLATIONS: Information published in a foreign language considered to merit NASA distribution in English.

TECHNICAL REPRINTS: Information derived from NASA activities and initially published in the form of journal articles.

SPECIAL PUBLICATIONS: Information derived from or of value to NASA activities but not necessarily reporting the results of individual NASA-programmed scientific efforts. Publications include conference proceedings, monographs, data compilations, handbooks, sourcebooks, and special bibliographies.

Details on the availability of these publications may be obtained from:

SCIENTIFIC AND TECHNICAL INFORMATION DIVISION

NATIONAL AERONAUTICS AND SPACE ADMINISTRATION

Washington, D.C. 20546